



Microstructure and fracture toughness of a WC-Fe cemented carbide layer produced by a diffusion-controlled reaction

Xiaolong Cai^{a,c,*}, Lisheng Zhong^{a,c,*}, Yunhua Xu^{a,b}, Xin Li^d, Mingxin Liu^e

^a School of Material Science and Engineering, Xi'an University of Technology, Xi'an 710048, China

^b YuLin University, YuLin 719000, China

^c Advanced Materials Analysis and Testing Centre, Xi'an 710048, China

^d Department of Electrical and Mechanical Engineering, Xi'an University of Architecture and Technology, Xi'an 710055, China

^e Humanities and Foreign Languages Institute, Xi'an University of Technology, Xi'an 710054, China

ARTICLE INFO

Keywords:

WC-Fe hardmetal layer
Grain morphology
Indentation method
Hardness
Fracture toughness

ABSTRACT

To improve the mechanical properties of the surface of iron-based alloys, a tungsten carbide-iron (WC-Fe) cemented carbide layer is produced on an alloy by adopting an isothermal annealing process, which was performed at 1050 °C for 4 h. By deeply etching the obtained sample, the morphologies of the WC ceramic grains in the WC-Fe hardmetal layer are characterized via scanning electron microscopy. The present results reveal three distinct morphologies consisting of rectangular, triangular prism and multi-layered shapes. Furthermore, the mechanical properties and fracture toughness of the WC-Fe layer are investigated through combined nanoindentation and Vickers indentation techniques. Nanoindentation testing is performed in a load range of 100 to 450 mN. Based on the data collected from the nanoindentation results, the average values of the hardness, Young' modulus and deformation ratio are evaluated, and the fracture toughness is determined to have a value of 3.08 MPa·m^{1/2} at 450 mN. In the Vickers indentation technique, however, by identifying the crack type and choosing the appropriate model, the fracture toughness is calculated to be 1.85–3.44 MPa·m^{1/2} at applied loads ranging from 0.98 to 4.9 N. The obtained fracture toughness results exhibit good consistence between the nanoindentation and Vickers indentation methods.

1. Introduction

Tungsten carbide (WC) ceramic, due to its attractive properties such as high melting point, good chemical stability and excellent resistance to wear, has been widely applied in cutting and drilling tools, petroleum pipelines and extrusion dies [1–5]. In general, WC ceramic is bound with such metals as Fe, Co and Ni by different preparation techniques to form hard metals or coatings on the surfaces of substrate materials [2,3,6–10]. Particularly, with respect to the production of WC-Fe cemented carbide layers on steel or iron substrates, a wide range of processes, which include plasma transferred arc metallurgical reaction [2], laser cladding [7,11] and magnetron sputtering [12,13], have been performed in recent studies. Although these processes exhibit a number of merits in the preparation of WC-Fe cermet coatings, their high cost may limit their applications. In this paper, a general and inexpensive in situ reaction process for producing a WC-Fe cemented carbide layer on the surface of an iron-based alloy is introduced. The obtained WC-Fe layer is expected to be applied in automobile disk

brakes. In our previous works [14–16], it was proven that the in situ reaction is a promising process through which carbide coatings or films, such as vanadium carbide, niobium carbide and tantalum carbide coatings, have been successfully prepared.

The ability of WC cermet coatings to resist wear and withstand deformation usually relies on an increase in hardness, but this strategy readily causes a decrease in the toughness. Therefore, the coordination of strength and toughness is a crucial requirement [17], which means that evaluation of both the fracture toughness and mechanical behaviours of WC cermet coating is very important because these properties are related to the reliability of the coatings in applications. A large number of studies have proven that the indentation technique can be used as a crucial technique to characterize the mechanical properties of micro-sized materials, such as ceramics, composites, coatings, cemented carbide layers, thin films and precipitate phases [13,18–23]. The indentation technique, including nanoindentation and Vickers indentation, is widely used to evaluate the hardness, Young' modulus, fracture toughness, creep and fatigue behaviour [4,9,13,17–23]. The

* Corresponding authors at: School of Material Science and Engineering, Xi'an University of Technology, Xi'an 710048, China.

E-mail addresses: xiaolongcai2015@163.com (X. Cai), zhonglisheng1984@163.com (L. Zhong).

<https://doi.org/10.1016/j.surfcoat.2018.10.096>

Received 28 May 2018; Received in revised form 4 August 2018; Accepted 30 October 2018

Available online 01 November 2018

0257-8972/ © 2018 Elsevier B.V. All rights reserved.

work conducted by F. Lofaj et al. [12] investigated stress evolution and cohesive cracking in a hard and stiff WC coating on a steel substrate through a combination of nanoindentation experiments and finite element modelling (FEM). A. Duszová et al. [19] determined the hardness and elastic modulus of individual phases as well as the influence of the crystallographic orientation of WC on the hardness and elastic modulus by the nanoindentation technique. In the work of Y. Gu et al. [22], a temperature-dependent fracture toughness model was proposed based on microcrack formation theory under Vickers indentation conditions. The fracture toughness of a WC-10Co4Cr coating/1018 steel substrate system was investigated by using this model, and the results showed an increase in toughness in a nonlinear manner. Although these researchers made use of the indentation technique to make considerable contributions to the characterization of the mechanical properties and fracture toughness of WC coatings, some challenges still remain.

In the previous studies [12,13,18–20,23], some challenges, such as the effects of the depth and area of indentation, crack morphology, residual stress and crystallographic orientation on the mechanical behaviour, were presented. In general, a Berkovich tip or Vickers indenter is commonly utilized on a hard, thin coating/soft ductile substrate system. Therefore, the depth and area of indentation have a strong influence on the measurement results. When the relative indentation depth has a maximum value > 10% of the coating thickness, the substrate inevitably has an effect on the mechanical properties of the coating [12]. Several different models for evaluating the fracture resistance have been proposed [23]. Based on the crack morphology, the fracture resistance can be accurately estimated by selecting a suitable available model. However, differences in the thermal expansion coefficients between the coating and the substrate can lead to the distribution of residual stress in the coating. Residual stress can influence the fracture toughness by promoting or inhibiting crack propagation [12,13]. A number of methods were adopted to address those challenges, and good advancements were made. However, in this research, one of the challenges is also explored by taking a combination of the results from the nanoindentation and Vickers indentation methods into consideration.

With respect to the WC-Fe cemented carbide layer, the size and morphology of the ceramic grains have a significant effect on the mechanical properties and fracture resistance. A number of previous works [7,24–29] described the morphology, growth and evolution of WC grains in coatings, composites, hardmetals and cemented carbides. However, the morphology of WC grains in coatings fabricated via an in situ reaction has seldom been reported. Consequently, the aim of this paper is to characterize the microstructure and evaluate the mechanical properties and fracture toughness of a WC cemented carbide layer produced at 1050 °C through isothermal annealing for 4 h.

2. Experimental procedure

2.1. Preparation of the WC-Fe cemented layer

The cemented tungsten carbide layer was fabricated on a cast iron (Fe) substrate by a solid-phase diffusion reaction during an isothermal annealing process. A pure tungsten plate (99.9%) and the Fe substrate were used to prepare the materials. The chemical composition of the substrate was 3.210 C, 0.077 P, 0.045 S, 0.240 Cr, 0.014 Cu, 1.050 Mn, 1.320 Si, and 94.044 Fe, in wt (%). The preparation procedure of the carbide layer was similar to that introduced in previous works [14–16,30]. According to the Fe-C-W ternary system [31], the process parameters of carbide layer production, including the annealing temperature and time, were selected to be 1050 °C and 4 h, respectively. Here, the aim of isothermal annealing was to facilitate the reaction between the W and C atoms to form a tungsten carbide phase. To clearly characterize the microstructure and avoid the effect of surface roughness on the results of the indentation measurements, the produced sample was ground by using Al₂O₃ abrasive papers ranging from 400 to

2000 mesh and subsequently polished by using a series of diamond pastes up to 0.5 µm.

2.2. Microstructural characterization

The phase compositions of the cross-section and surface of the cemented carbide layer were determined with an X-ray diffractometer (XRD)-7000 (Shimadzu, Japan) with Cu K α radiation at 40 kV and 40 mA in the 2 θ range of 20–90°. The microstructure of the carbide layer was characterized by using a scanning electron microscope (SEM, VEGA3LMH TESCAN, Brno). Further, to observe the morphologies of the tungsten carbide grains, chemical corrosion and extraction processes were performed. First, the obtained sample was etched in a 25% hydrochloric acid solution for 36 h until the substrate was dissolved. Second, the remaining tungsten carbide ceramics were divided into two parts: one portion consisted of the ceramic grains adhered to the thin tungsten plate, and the other consisted of the ceramic grains that floated in an alcoholic solution. The former portion was cleaned with absolute ethyl alcohol and then dried to obtain the specimen. In contrast, the latter was extracted to obtain tungsten carbide powders. Third, through SEM experiments, the morphologies of the tungsten carbide grains were characterized.

2.3. Nanoindentation

Nanoindentation testing was performed on a Nanoindenter G200 (Agilent, Oak Ridge, USA) by using a diamond Berkovich tip in load-controlled measurement mode with applied loads of 100, 200, 300, 400, and 450 mN. A Poisson's ratio of 0.25 was performed for the carbide layer. Moreover, some details of the testing conditions can be found in the literature [30]. The final values of the hardness and Young's modulus were obtained by performing nanoindentation tests on the cross-section of the layer, in which the average value of 3 tests conducted at different locations is reported. The deformation behaviours of the tungsten carbide layer exhibiting elastic deformation and plastic deformation related to the load-bearing capacity during the loading and unloading process were estimated by expression (1) [30,32]:

$$\Delta p = (h_r/h_{\max}) \times 100\% \quad (1)$$

where Δp is the plastic deformation ratio, h_{\max} is the maximum depth, and h_r is the residual depth in the load-displacement curve. Additionally, the indentation topographies and crack propagation were investigated by using SEM. The crack length at the corner of the indentation was measured by averaging the results of 3 tests. Based on the values of hardness, Young's modulus and crack length obtained from the nanoindentation method, with respect to the Palmqvist crack system, the fracture toughness (K_{IC}) of the layer was calculated by the following equation [33]:

$$K_{IC} = k \left(\frac{a}{l} \right)^{\frac{1}{2}} \left(\frac{E}{H} \right)^{\frac{2}{3}} \frac{P}{C^{\frac{3}{2}}} \quad (2)$$

where H is the hardness (GPa), E is the Young's modulus (GPa), P is the load applied (N), k is a constant ($k = 0.016$ for the Berkovich indenter), and C is the total length of a and l , where a and l are the half diagonals of the indentation imprint and the crack length, respectively.

2.4. Microindentation

Microindentation as a simple and convenient technique was also used to evaluate the microhardness (H_{HV}) and fracture resistance [23,34]. To have a better understanding of the fracture resistance of the WC-Fe cemented layer, the K_{IC} value determined from the Vickers indentation methods was also performed. To acquire the mean values of H_{HV} and K_{IC} , the cross-section of the layer was examined by a Vickers indenter (MC010-HV-1000) at normal loads of 0.98, 1.96, 2.94 and

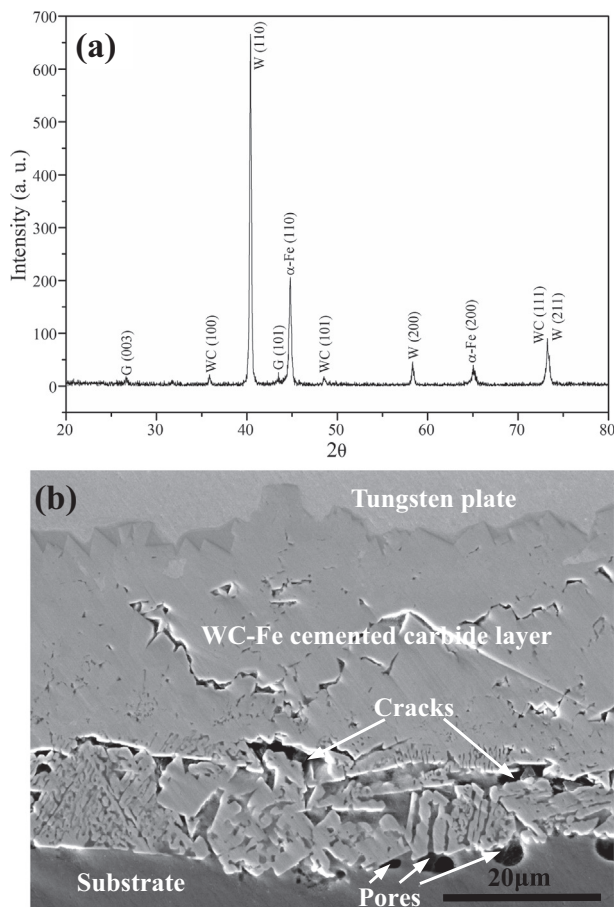


Fig. 1. (a) Cross-sectional XRD pattern of the specimen and (b) SEM image of the carbide layer obtained from reaction at 1050 °C for 4 h.

4.9 N applying at least 3 indentations. With the Vickers indenter, the fracture toughness K_{IC} could be evaluated by the following equation [34]:

$$K_{IC} = 0.024 \left(\frac{E}{H_{HV}} \right)^{\frac{1}{2}} \frac{P}{C^{\frac{3}{2}}} \quad (3)$$

where H_{HV} is the Vickers indentation hardness and the other parameters, such as C and P , are consistent with those mentioned above for Eq. (2).

3. Results and discussion

3.1. Microstructure and phase composition

The microstructure and phase composition of the sample cross-section are displayed in Fig. 1. The XRD analysis shows that the diffraction patterns of the sample cross-section (Fig. 1a) consist of graphite (G), ferrite (α-Fe), tungsten (W) and tungsten carbide (WC) phases. Among those phases, the G and α-Fe phases originate from the iron alloy substrate because it contains flake graphite and ferrite [15,16]. The appearance of the metal W phase is attributed to residual tungsten plate, indicating that the in situ reaction occurring during the annealing process was incomplete. The microstructure of the sample cross-section is shown in Fig. 1b, where a relatively compact cemented carbide layer with a thickness of approximately $45.87 \pm 1.67 \mu\text{m}$ is clearly visible between the tungsten plate and substrate. Additionally, it is evident that some defects, such as pores and cracks, are present in the layer cross-section and substrate. Effect of the isothermal heating on the substrate is that it leads to occurrence of decarburization in the

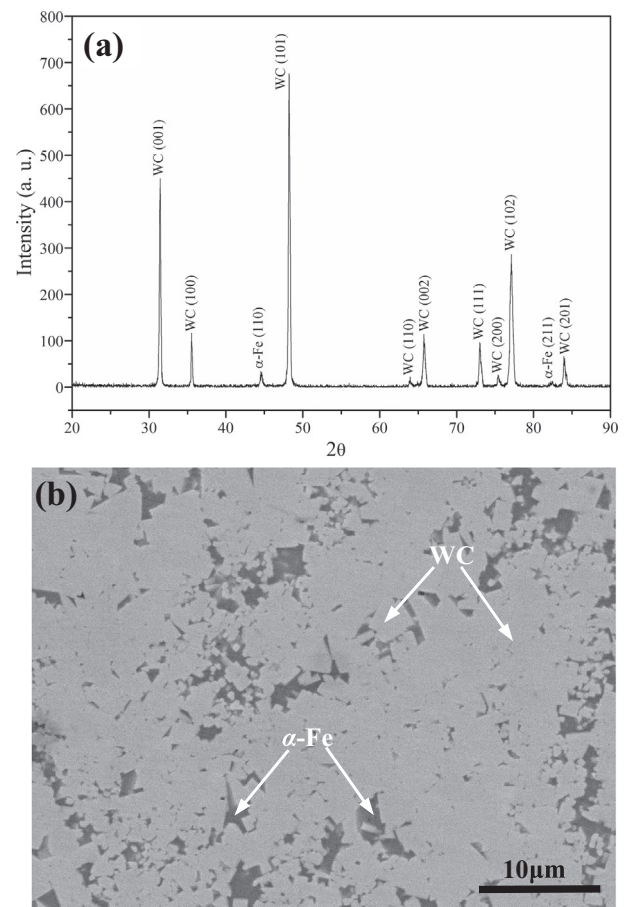


Fig. 2. (a) XRD pattern and (b) SEM micrograph of the carbide layer surface.

substrate close to the layer. Therefore, it is considered that those pores existing in the interface of the layer/substrate are a consequence of decarburization resulting in consumption of graphite phase during ISR process. Cracks in the layer may be caused by residual stress from the machining or cooling of the sample. Further details of the microstructure and phase composition of the carbide layer surface are displayed in Fig. 2. As illustrated in Fig. 2a, the XRD pattern of the surface layer contains only two weak α-Fe diffraction peaks, and the other stronger diffraction peaks correspond to WC reflections. The XRD results are in good agreement with those of the prior works [2,6,9,11]. Fig. 2b indicates that the WC phase dominates the microstructure of the layer. A similar microstructure can be found in similar cemented carbides [9,18,19,26] reported previously. According to the XRD and SEM results (Figs. 1 and 2) obtained, the phase composition of the cemented carbide layer has been confirmed, and it is comprised of a dominant WC ceramic phase and a small amount of α-Fe phase.

In the present study, the formation of the WC phase depends strongly on the diffusion and reaction of C and W atoms in the solid state during the annealing process. Therefore, the growth of the cemented WC-Fe layer is also related to the diffusion and reaction of C and W atoms. To better investigate the growth of the WC-Fe hardmetal layer, the following acceptable assumptions are proposed: (i) the diffusion of C and W atoms can take place at the annealing temperature, (ii) C atom diffusion occurs perpendicular to the tungsten plate, and W atom diffusion occurs in the opposite direction and (iii) once contact occurs between the C and W atoms, the reaction can happen quickly. Based on those abovementioned assumptions, it can be inferred that the kinetics of the reaction of C and W atoms is remarkably faster than that of the diffusion of C and W atoms in the carbide layer. Thus, the reaction of C and W depends on their supply by the diffusion, which

indicates that the diffusion kinetics is a key aspect for the formation of the carbide layer. Similarly, the growth kinetics of titanium boride layers was created by solid-state boron diffusion at a titanium surface [35]. Hence, from this point of view, the influence of the reaction kinetics on WC-Fe cemented carbide layer growth is not considered in further discussions. With respect to diffusion, as it is known that the C atom radius (0.091 nm) is smaller than the W atom radius (0.202 nm), the C diffusion ratio is significantly faster than the W diffusion ratio in the carbide layer [36]. Taking this factor into consideration, it is worth pointing out that the contribution of C atom diffusion to the cemented WC-Fe layer growth is predominant. Due to the fact that C atom diffusion occurs perpendicular to the tungsten plate, the tungsten plate/tungsten carbide interface also migrates in the direction of the tungsten plate. This process can lead to growth of the layer perpendicular to the tungsten plate.

Depending on the carbon content of the substrate materials, tungsten carbide phases of different types can be obtained. With respect to the formation of tungsten carbide, a previous study [37] reported that the C concentration is required to be approximately 3.0 wt% and 6.13 wt% for the synthesis of W_2C and WC, respectively. In another work, a tungsten carbide coating deposited on a 12,050 steel substrate consisted of only the WC phase [12,13]. Similarly, the phase composition of the carbide coatings formed on the surface of an Fe-based alloy [2,27] or AISI 304 stainless steel [38] contained WC and M_6C but no W_2C phase. However, it was reported that in addition to the WC phase existing in similar carbide composite coatings, the W_2C phase also formed on the surfaces of A3 mild steel [7] and 304 stainless steel [11] in the W-rich zone. In the present study, the carbon content of the Fe substrate has a value of approximately 3.2 wt%, which is slightly higher than that of other reported steel or iron substrates [2,7,11,12,27,38]. The WC phase is observed in the XRD pattern, whereas the W_2C phase is not. Through comparison of the results with those of previous works, it can be concluded that the difference in carbide types obtained may be a consequence of differences in the chemical composition of the substrate. Additionally, the difference in phases is associated with the process parameters adopted, such as the temperature and time.

3.2. Grain morphology

To reveal the morphology, the WC ceramic grains that adhered to the thin tungsten plate were uncovered by deeply etching the sample using a 25% hydrochloric acid solution. The features of the layer surface after etching are displayed in Fig. 3. Only WC ceramic grains are observed due to dissolution of the α -Fe phase (Fig. 3a). Fig. 3b shows that the SEM morphologies of the in situ-grown WC grains consist of rectangular and triangular prism shapes. More detailed analysis of the morphology can be found in Fig. 4. An individual WC grain with a thickness of 1.64 μ m, length of 10.47 μ m and width of 7.13 μ m showing

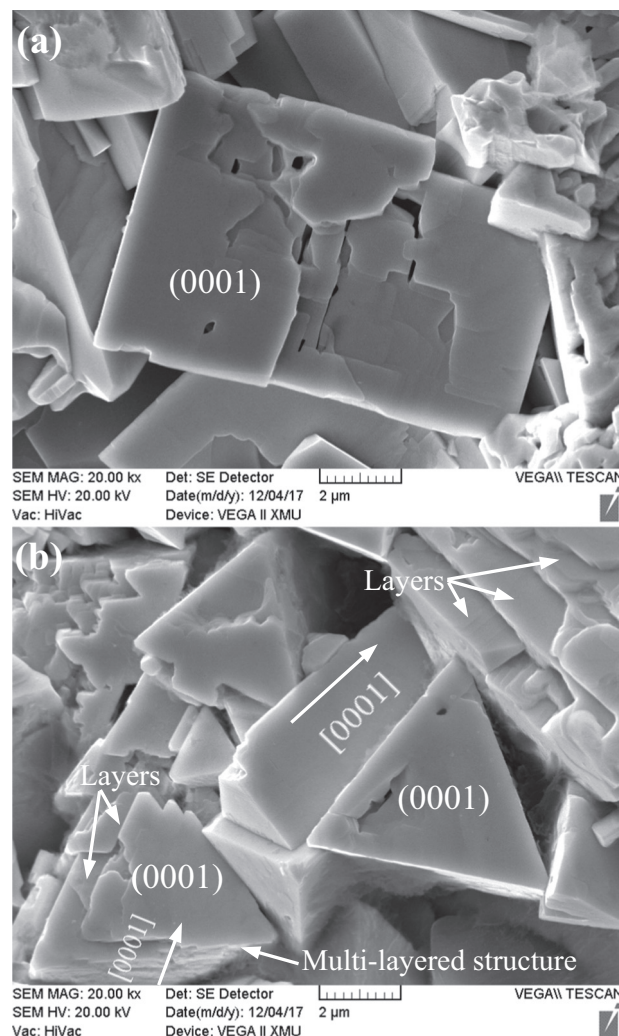


Fig. 4. The morphology of the WC particles obtained after acid etching: (a) rectangular shape and (b) triangular prisms and multi-layered structure.

the (0001) lattice plane and a rectangular shape can be clearly observed in Fig. 4a. This result of the WC grain morphology is consistent with the results reported by several researchers [9,18,19,39]. Fig. 4b illustrates the triangular prism shape and also shows that the (0001) plane and [0001] direction are involved in the WC grains. In addition, a layer-by-layer (multi-layered) structure is found in the WC grain in Fig. 4b. Both the triangular prisms and multi-layered structures are akin to the WC morphologies reported in several investigations [27–29,39]. The former

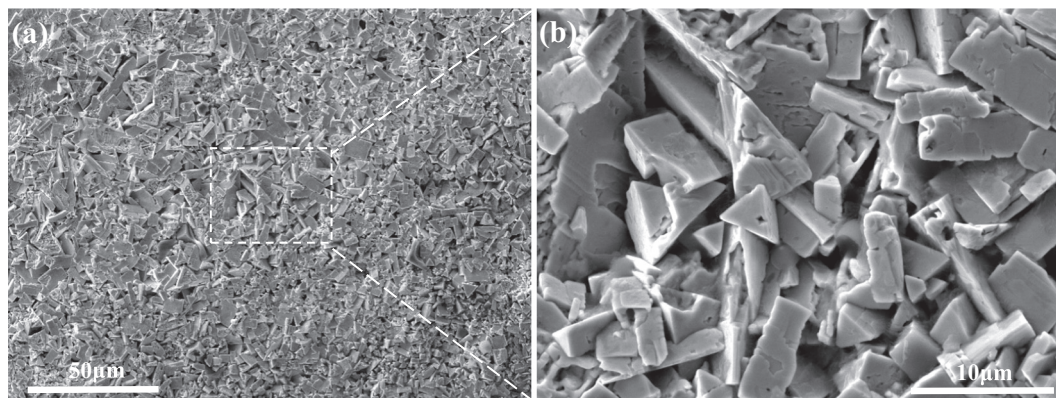


Fig. 3. (a) SEM micrograph of the carbide layer surface after deep etching and (b) magnified SEM image of the region marked in (a).

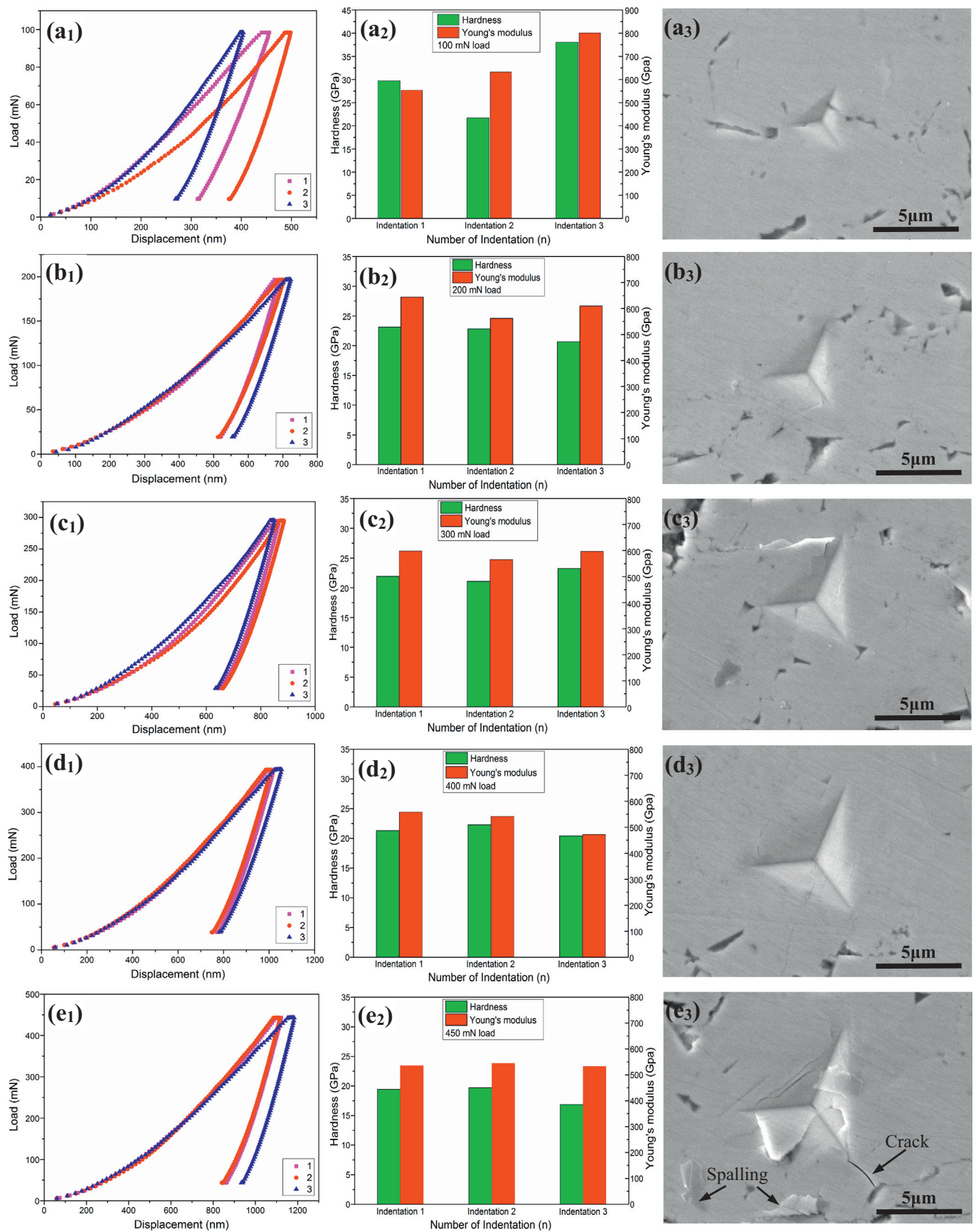


Fig. 5. (a₁), (b₁), (c₁), (d₁) and (e₁) Load-displacement curves, (a₂), (b₂), (c₂), (d₂) and (e₂) hardness and Young's modulus distributions, and (a₃), (b₃), (c₃), (d₃) and (e₃) nanoindentation imprints of the WC-Fe hardmetal layer under loads in the range from 100 to 450 mN.

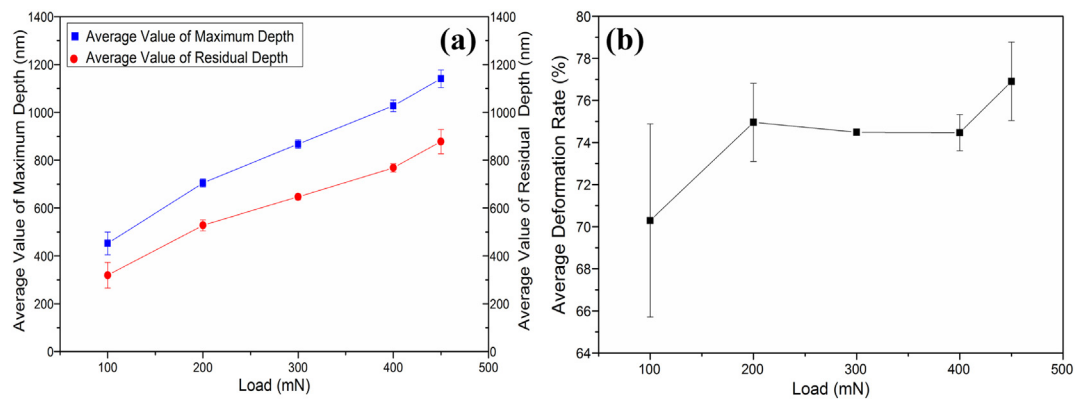


Fig. 6. (a) Average values of the maximum depth and residual depth and (b) the variation in the average deformation ratio under different loads.

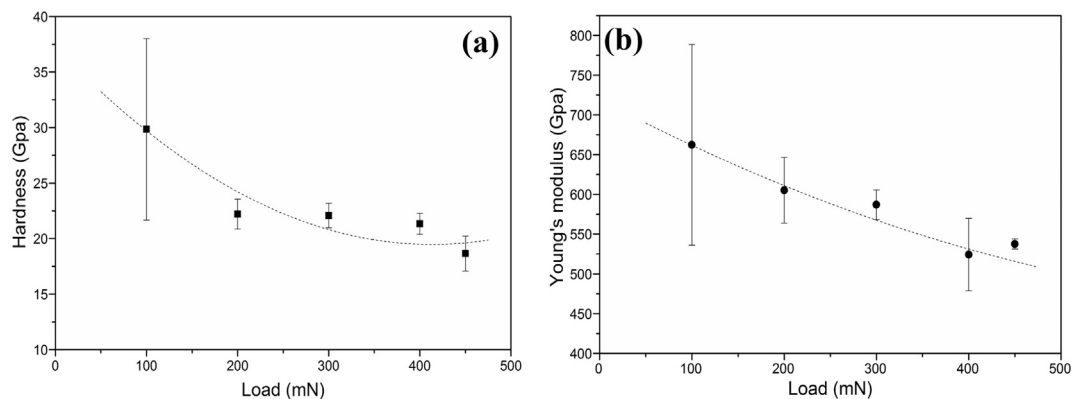


Fig. 7. Variations in the (a) hardness and (b) Young's modulus with different applied loads in the nanoindentation measurements.

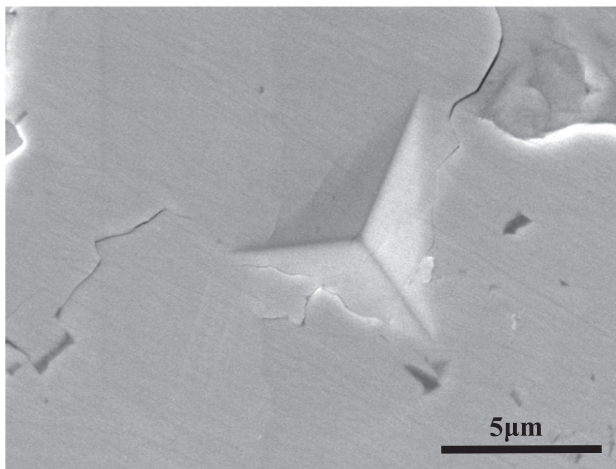


Fig. 8. Details of a nanoindentation imprint generated under a load of 450 mN.

is considered to be the equilibrium shape of WC due to its more stable surface energy [27], and the formation of the latter can occur through 2D nucleation and 2D or 3D growth [28,29]. Individual WC nucleation and growth process occur on the (0001) plane, and moreover, WC growth is accompanied by layer-by-layer stacking along the [0001] direction. In the previous studies [4,28,29], a rounded morphology was reported for the WC grains, but this morphology is not observed in the present study. The variations in the morphology of the individual WC grains is related to their growth, which relies considerably on the process parameters, particularly the temperature [25,29], because the surface energy of the crystal facet can be influenced by those parameters. Crystal growth is related to its surface energy. Due to the

difference in the surface energies of the crystal facets, the occurrence of competitive growth between crystal facets results in different growth rates [27]. According to crystal growth theories, the grown crystal morphology is dominated by the slow-growing facets because the fast-growing facets may disappear and not be represented in the final crystal [40]. Additionally, Yang Zhong et al. [41] reported that alloying elements, such as Co and Ni, have a remarkable effect on the WC morphology by changing the dimensions of its surface facets. Therefore, it is possible that the presence of WC grains in this study was also influenced by the Fe present in the carbide layer during the isothermal annealing process. A prime reason for this effect is that Fe has a catalytic effect and can increase the diffusivity of W and C in between WC particles [25].

As discussed above, the morphology of the WC particles was determined to consist mainly of rectangular, triangular prism and multi-layered structures by a SEM testing method. Here, it should be noted that the shape of the WC particles can influence the mechanical behaviour of the material. Consequently, to examine the mechanical properties of the formed tungsten carbide layer containing WC particles with different shapes, further investigation was carried out by using the indentation technique.

3.3. Mechanical properties determined by nanoindentation

By using nanoindentation measurements, the main mechanical properties, including the nanohardness (H), Young's modulus (E), fracture toughness (K_{IC}) and creep and fatigue behaviours, can be determined [18–20,30]. In the present study, however, nanoindentation was carried out to investigate the influence of various loads on the H and E values of the WC-Fe cemented carbide layer, and then the acquired data were applied in the evaluation of K_{IC} . Fig. 5 shows the nanoindentation measurement results, including the hardness, Young's

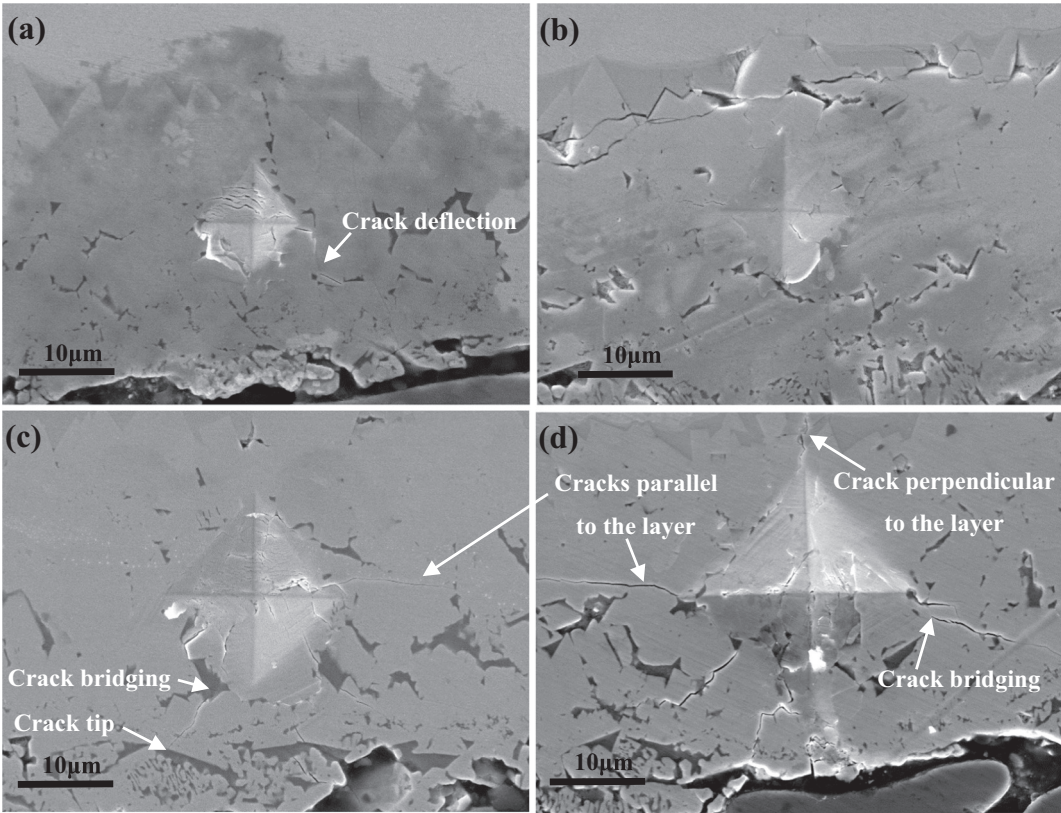


Fig. 9. Morphologies of the Vickers indents generated at loads of (a) 0.98, (b) 1.96, (c) 2.94 and (d) 4.9 N.

Table 1
Lengths and directions of the cracks generated in the Vickers indentation method from 0.98 to 4.9 N.

Applied loads (g)	Crack 1 (0°)		Crack 2 (0°)		Crack 3 (90°)		Crack 4(90°)	
	a ₁ (μm)	L ₁ (μm)	a ₂ (μm)	L ₂ (μm)	a ₃ (μm)	L ₃ (μm)	a ₄ (μm)	L ₄ (μm)
100	5.19	8.29	~	~	~	~	~	~
200	6.88	6.81	7.83	9.21	9.04	4.94	9.04	5.66
300	9.54	15.13	9.54	13.19	9.84	9.26	9.84	9.48
500	13.90	21.69	12.48	17.19	13.38	10.43	14.42	6.93

moduli, load–displacement curves and indentation impressions, for the WC-Fe layer cross-section obtained at applied loads of 100, 200, 300, 400 and 450 mN. To obtain reliable measurement data, the nanoindentation experiment was performed at least three times for each load. Comparison of the load-displacement curves clearly indicates that the displacement depth increases with increasing load from 100 mN to 450 mN, as shown in Fig. 5a₁, b₁, c₁, d₁ and e₁. Furthermore, the load-displacement curves under all the loads except for 100 mN are relatively well superimposed, suggesting that the acquired experimental results have a high accuracy. With regard to the 100-mN load, due to the small contact area between the indenter and the carbide layer under this condition, the presence of defects, such as pores and crack (Figs. 1b and 5a₃), in the layer has a strong effect on the experimental measurement and thus leads to greater deviation in the results. It is universally acknowledged that the ability of a material, particularly a hard material, to undergo limited deformation is a key aspect of its toughness because this feature enables the local dissipation of high stresses that would cause the material to fracture [17]. Therefore, the deformation behaviour of the WC-Fe hardmetal layer was investigated before evaluating the fracture toughness. Based on the above load-displacement curve results, average values of the maximum indentation depth (MID) and residual indentation depth (RID) at different loads were calculated, as depicted in Fig. 6a. Further, on the basis of Eq. (1) and the average

values of the MID and RID, the variation in the deformation ratio of the WC-Fe layer under various loads was calculated, and the result is shown in Fig. 6b, where an increasing trend can be found.

Furthermore, the role of nano-indentation size is important for mechanical properties, because it could be possible to indent Fe-rich regions and single WC grains in the layer structure. With respect to the former, it presents higher toughness and lower strength. However, the latter shows an opposite case. A change in the deformation behaviour with increasing load can be observed, and a crack is generated at the corner of the indentation when the load reaches 450 mN, as shown in Fig. 5a₃ to e₃. Moreover, it is found that lamellar fragments formed from spalling around the indentation. A probable reason for the presence of the lamellar fragments is that the surface of the multi-layered WC grain was subjected to the Berkovich tip. This leads to spalling of the topmost surface layer on the multi-layered structure. Obviously, the layer undergoes deformation and does not fracture when the load is below 450 mN, and above this value, fracture could be observed. Additionally, the distributions of the hardness and Young' modulus are plotted in Fig. 5a₂ to e₂, and based on the gathered data, their average values were calculated, as presented in Fig. 7. The values of both the hardness and Young' modulus exhibit a decreasing trend with an increase in the load. However, a simple comparison shows a decrease of 37% in *H* and 19% in *E* when the load attains 450 mN, indicating that

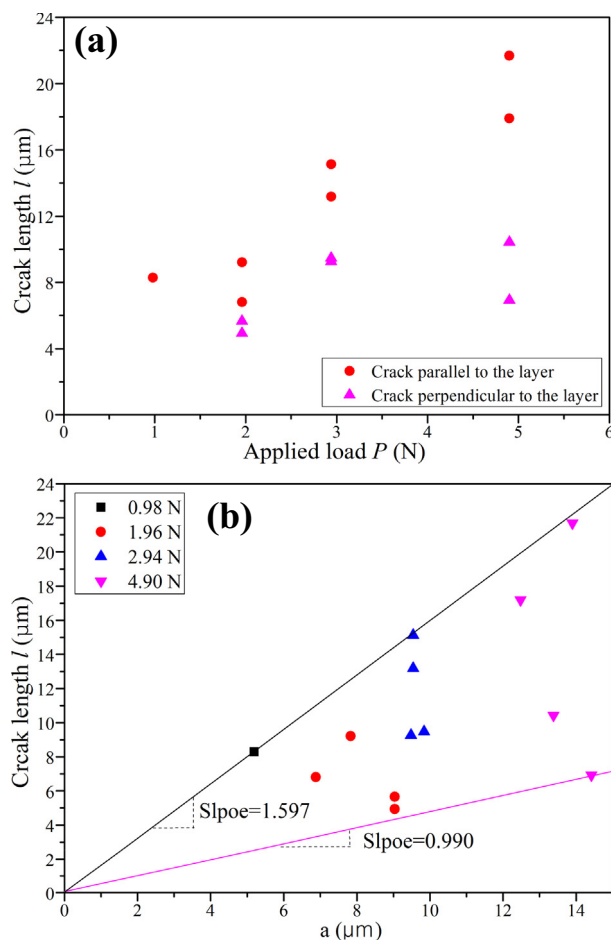


Fig. 10. (a) Crack length l as a function of the applied load and (b) relation between the value of l/a and the load.

the decrease in H is substantially larger than the decrease in E . Numerous researchers regard this phenomenon of H decreasing with increasing load as the indentation size effect (ISE) [18,23,42], which has a strong influence on the precise evaluation of the mechanical properties, especially the fracture toughness. Under the nanoindentation method, the fracture toughness of the WC-Fe carbide layer was determined at only 450 mN, at which fracture occurred. As illustrated in Fig. 8, the fracture morphology of the layer at a load of 450 mN was examined. Generally, there are numerous models related to the evaluation of a hard material's toughness in indentation method, but the applicability of which strongly depends on the crack type generated. Taking this factor into consideration, according to the collected data, a ratio of l/a with an average value of approximately 1.49 ± 0.103 was obtained, which lies in the range of $1 < l/a < 2.5$ set by Niihara et al. [33,43] and thus, the crack belongs to the Palmqvist crack system. Therefore, Eq. (2) was selected as the appropriate model for calculating the toughness of the layer at a load of 450 mN. By applying the average values of the crack length l , H and E in Eq. (2), the mean value of K_{IC} was determined to be $3.08 \text{ MPa}\cdot\text{m}^{0.5}$ for the WC-Fe layer. This value is in a good agreement with the fracture toughness ($K_{IC} = 3.50 \text{ MPa}\cdot\text{m}^{0.5}$) of the WC coating on a steel substrate measured by nanoindentation [13].

As discussed above, the mechanical properties of the WC-Fe cemented carbide layer have been characterized under the nanoindentation condition. However, the dependence of the fracture toughness of the layer on the applied load is not presented here. In general, the presence of a Palmqvist crack system takes place in two cases: one is for a tough material at a high load and the other is for a brittle material at a low load. With respect to the carbide layer, when the applied load is

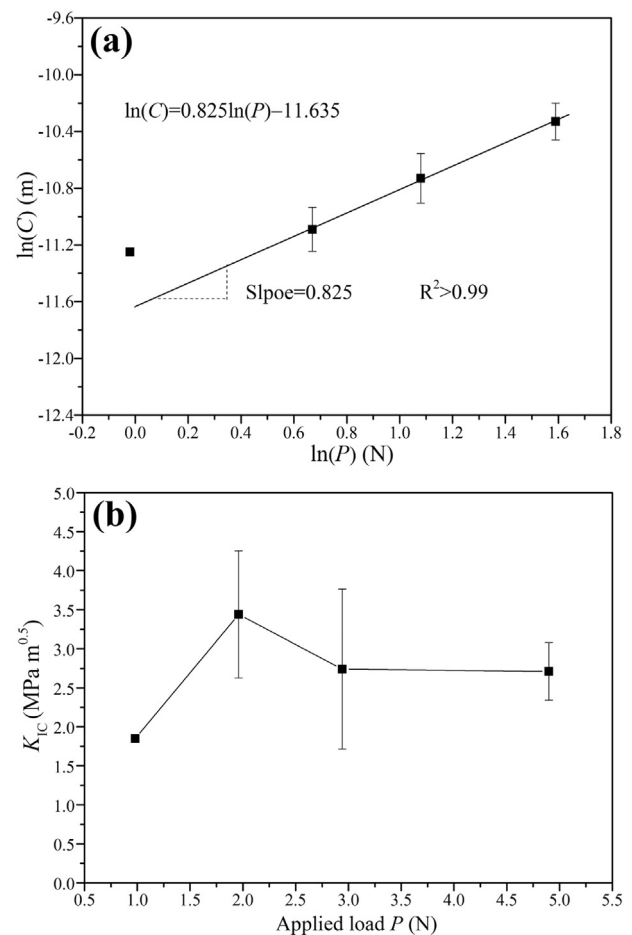


Fig. 11. (a) Plot of $\ln(C)$ as a function of $\ln(P)$ and (b) the dependence of the fracture toughness on the applied load under Vickers indentation.

increased, the type of crack system may change, which suggests that K_{IC} needs to be estimated again by adopting the appropriate equation. Accordingly, microindentation experiments were carried out.

3.4. Fracture toughness determined by microindentation

The Vickers indentation method, a simple and highly efficient technique, is usually used to investigate the fracture toughness, especially with regard to WC coatings [3,5,22,38]. In the present study, the relationship between various loads and the fracture behaviour was analysed by using the Vickers indentation method. Fig. 9 shows the evolution in the fracture feature of the layer under various loads. It can be observed that all the crack lengths and the crack quantity increase with the applied load, and crack deflection is presented. The microstructural defects such as the presence of cracks and pores in the surface layer lead to stress concentration around them. When the layer is subjected to the applied load, in order to release energy, some regions with high stress appear cracking. In general, to maintain the driving force of the crack propagation, the crack tends to extend towards the high stress regions. Therefore, under the applied load, the crack easily occurs deflection (Fig. 9a) during propagation due to the heterogeneity of defects distribution. Additionally, crack bridging also is found and crack tip ends at a ductile phase (α -Fe), as shown in Fig. 9c and d. α -Fe as a bridge contributes to the toughness via plastic dissipation [30]. Due to the existence of some pores and thermal stress at the interface of WC-Fe layer/substrate, under a high load of 4.9 N, the interface occurs the cracking (Fig. 9d), which results in a reduction in the cohesion of the layer to the substrate. Table 1 illustrates the dependence of the crack length on the applied load. It is worthwhile to note that the length of

Table 2
Microhardness of the WC-Fe hardmetal layer determined using a Vickers indenter at four different loads.

Indentation load (g)	100	200	300	500
Vickers hardness (GPa)	16.1 ± 0.11	13.2 ± 0.54	14.1 ± 0.34	12.87 ± 0.97

the crack parallel to the layer is greater than that of the crack perpendicular to the layer (Fig. 9d), as depicted in Fig. 10a. This situation can be caused by the distribution of residual stress, which is associated with the thermal expansion coefficients of the diverse phases. There is an essential difference in the thermal expansion coefficients between the W and WC phases, which have values of $4.5 \times 10^{-6}/\text{K}$ and $6.9 \times 10^{-6}/\text{K}$, respectively. In contrast, the thermal expansion coefficient of cast iron ranges from $9.2 \times 10^{-6}/\text{K}$ to $11.8 \times 10^{-6}/\text{K}$. After the sample was cooled, this distribution of the thermal expansion coefficients created compressive stress in the vicinity of the interface between the W plate and the WC-Fe layer in addition to tensile stress around the interface between the WC-Fe layer and substrate. The former can inhibit crack propagation by diminishing the shear stress generated through the applied load and narrowing the crack opening. In contrast, the latter can promote crack propagation by enhancing the shear stress effect. Furthermore, the presence of the tungsten plate could influence the mechanical properties of the surface layer, especially the fracture toughness. As a ductile phase, when the crack tip encounters it, the crack terminates on it. Such a situation can increase the toughness of the layer. Accordingly, considering the influence of both abovementioned stresses on the fracture toughness measurement, the cracks parallel to the WC-Fe layer were adopted to calculate the toughness here.

Numerous models and equations that relate the degree of cracking to the fracture toughness have been reported in the literature [44]. On the basis of the crack type, those models are classified into two categories: (i) the radial Palmqvist crack model and (ii) the radial-median or halfpenny-shaped crack model. Several equations related to the fracture toughness calculation have been derived according to those models. Therefore, the judgement of the crack type is crucial for applying the appropriate equations. The variation in l/a is plotted in Fig. 10b, and the fact that the l/a values are in the range of 0.99 to 1.597 provides strong evidence that the formed cracks belong to the Palmqvist crack system. To further confirm that fact, the proportionality of $\ln C$ to $\ln P$ was obtained for the layer, as plotted in Fig. 11a. In general, if the slope of the plot of $\ln C$ as a function of $\ln P$ is approximately 0.66, the cracks can be considered to belong to the radial-median system. Here, it can be observed that the obtained slope possesses a value of 0.825, which is evidently larger than 0.66, further confirming that the formed cracks belong to the Palmqvist crack system. For the Palmqvist crack model, Eq. (3) was selected from numerous equations [23,34,44] to calculate the toughness. Based on Eq. (3), the Young's modulus obtained from the nanoindentation method (537.61 ± 6.232) and the microhardness determined by the Vickers indenter (Table 2), the value of K_{IC} was calculated. Fig. 11b shows the dependence of K_{IC} on the applied loads under the Vickers indentation method. An increasing trend occurs during the initial state, and then the value decreases and achieves a steady state with an increase in the load. The calculated K_{IC} value varies in the range of $1.85\text{--}3.44 \text{ MPa}\cdot\text{m}^{1/2}$, which is two times smaller than the value of $8.77 \pm 0.61 \text{ MPa}\cdot\text{m}^{1/2}$ obtained by three-point bending (TPB) [45]. Because of the somewhat empirical nature of the indentation fracture method, differences exist between the K_{IC} values determined by this method and by the conventional fracture toughness methods, such as TPB or chevron notch [45].

D. Wang et al. [3] reported that K_{IC} results obtained by indentation of three representative types of WC-CoCr coatings with diverse compositions were $4.97 \pm 0.32 \text{ MPa}\cdot\text{m}^{1/2}$, $6.03 \pm 0.19 \text{ MPa}\cdot\text{m}^{1/2}$ and $7.12 \pm 0.13 \text{ MPa}\cdot\text{m}^{1/2}$. The average K_{IC} value of the WC-Co coating determined by using the Vickers indentation method was

$11.5 \pm 1.4 \text{ MPa}\cdot\text{m}^{1/2}$, which is higher than that of conventional coating [5]. For any material, the intrinsic toughness should have a certain value. However, those differences in the K_{IC} values are mainly attributed to the testing conditions and the microstructure [23,34]. It is well known that the formation of cracks is sensitive to the presence of defects and stress [17]. On one hand, the WC-Fe cemented carbide layer contains a number of microcracks and pores (Fig. 1b), which can cause stress to concentrate around them. The existence of stress concentration in the layer increases the crack-driving force and thus accelerates the initiation and propagation of the crack, which leads to a reduction in the K_{IC} value. On the other hand, a small amount of the α -Fe phase and WC grains with rectangular, triangular prism and multi-layered shapes constitute the WC-Fe cemented layer. Thus, the diverse morphologies of the WC grains may influence the hardness and toughness of the layer. Several studies [27,29] reported that a plate-like WC structure (high aspect ratio) can simultaneously increase the hardness and toughness and that the triangular prisms (low aspect ratio) have a smaller contribution to the toughness. However, it can be observed that the triangular prism shape plays a dominant role in the carbide layer (Fig. 3). Therefore, it is evident that the morphology of the WC grains is an important factor that influences the K_{IC} value. Additionally, Fig. 1b reveals that the surface layer displays an inhomogeneity in composition. Obviously, the content of α -Fe phase decreases with distance from the Fe-rich interface. This inhomogeneous structure can influence the H , E and fracture toughness results. In the present study, the mean value of K_{IC} calculated by using the Vickers indentation method lies in the range of $1.85\text{--}3.44 \text{ MPa}\cdot\text{m}^{1/2}$, which matches with the result ($3.08 \text{ MPa}\cdot\text{m}^{1/2}$) determined by using the nanoindentation method. Thus, the K_{IC} value calculated for the WC-Fe carbide layer by a combination of the nanoindentation and Vickers indentation methods is concluded to be reasonable.

4. Conclusions

To improve the surface strength of iron-based alloys, a WC-Fe cemented carbide layer was fabricated by adopting an isothermal annealing process. The WC-Fe carbide layer formed as a consequence of a diffusion-controlled reaction in the solid state. The morphology of the obtained WC particles was characterized. Rectangular, triangular prisms shapes as well as a multi-layered structure were clearly observed. In addition, a multi-layered structure grew along the [0001] direction.

The nanoindentation results for the WC-Fe carbide layer provided mean values of $18.661 \pm 1.569\text{--}29.842 \pm 8.168 \text{ GPa}$ and $537.611 \pm 6.232\text{--}662.225 \pm 126.255 \text{ GPa}$, respectively, for the nanoindentation and Young's modulus with the various loads from 100 mN to 450 mN. When the load was 450 mN or greater, fracture could occur. Thus, under the nanoindentation method, the calculated fracture toughness had a mean value of $3.08 \text{ MPa}\cdot\text{m}^{1/2}$ at a load of 450 mN.

Under Vickers indentation testing, the generated cracks belonged to the Palmqvist crack category, and the average fracture toughness value of the WC-Fe cemented carbide layer was determined to be within the range of $1.85\text{--}3.44 \text{ MPa}\cdot\text{m}^{1/2}$, in which an increasing trend occurred during the initial state, and the value then decreased and achieved a steady state with an increase in the applied load.

Acknowledgements

The authors are grateful for the support of the Doctoral Innovation Fund (No. 310-252071703) and the Projects of Shaanxi Provincial Key

Research (Nos. 2017ZDXM-GY-032 and 2017ZDXM-GY-043).

References

- [1] P. Gao, Z. Liang, X. Wang, et al., Cutting edge damage in grinding of cemented carbides micro end mills, *Ceram. Int.* 43 (2017) 11331–11338.
- [2] Y. Yuan, Z. Li, Microstructure and tribology behaviors of in-situ WC/Fe carbide coating fabricated by plasma transferred arc metallurgical reaction, *Appl. Surf. Sci.* 423 (2017) 13–24.
- [3] D. Wang, B. Zhang, C. Jia, et al., Influence of carbide grain size and crystal characteristics on the microstructure and mechanical properties of HVOF-sprayed WC-CoCr coatings, *Int. J. Refract. Met. Hard Mater.* 69 (2017) 138–152.
- [4] J.-C. Han, M. Jafari, C.-G. Park, Jae-Bok Seol, Microstructure-property relations in WC-Co coatings sprayed from combinatorial Ni-plated and nanostructured powders, *Mater. Charact.* 129 (2017) 207–216.
- [5] P. Mi, T. Wang, F. Ye, Influences of the compositions and mechanical properties of HVOF sprayed bimodal WC-Co coating on its high temperature wear performance, *Int. J. Refract. Met. Hard Mater.* 69 (2017) 158–163.
- [6] In-Jin Shon, In-Kyoon Jeong, In-Yong Ko, Jung-Mann Doh, Kee-Do Woo, Sintering behavior and mechanical properties of WC-10Co, WC-10Ni and WC-10Fe hard materials produced by high-frequency induction heated sintering, *Ceram. Int.* 35 (2009) 339–344.
- [7] S. Zhou, X. Zeng, Growth characteristics and mechanism of carbides precipitated in WC-Fe composite coatings by laser induction hybrid rapid cladding, *J. Alloys Compd.* 505 (2010) 685–691.
- [8] C. Buchegger, W. Lengauer, J. Bernardi, et al., Diffusion parameters of grain-growth inhibitors in WC based hardmetals with Co, Fe/Ni and Fe/Co/Ni binder alloys, *Int. J. Refract. Met. Hard Mater.* 49 (2015) 67–74.
- [9] E.A. Alvarez, C.G. Oliver, F. Soldera, J.L. García, Densification and FIB, SEM, TEM microstructures of WC composites with Fe or Co matrices, *Proc. Mater. Sci.* 8 (2015) 406–413.
- [10] Ling-jun Guo, J. Peng, G. Kou, Guo-ge Shi, Kai-yuan Dong, Oxyacetylene torch ablation resistance of Co-modified WC coating deposited on C/C composites by supersonic atmosphere plasma spraying, *Ceram. Int.* 43 (2017) 8989–8998.
- [11] J. Wang, L. Li, W. Tao, Crack initiation and propagation behavior of WC particles reinforced Fe-based metal matrix composite produced by laser melting deposition, *Opt. Laser Technol.* 82 (2016) 170–182.
- [12] František Lofaj, Dušan Németh, Multiple cohesive cracking during nanoindentation in a hard W-C coating/steel substrate system by FEM, *J. Eur. Ceram. Soc.* 37 (2017) 4379–4388.
- [13] T. Csanádi, D. Németh, F. Lofaj, Mechanical properties of hard W-C coating on steel substrate deduced from nanoindentation and finite element modeling, *Exp. Mech.* 57 (2017) 1057–1069.
- [14] X. Cai, L. Zhong, Y. Xu, Z. Lu, J. Li, J. Zhu, Y. Ding, H. Yan, Microstructural characterization of a V_2C and V_8C_7 ceramic-reinforced Fe substrate surface compound layer by EBSD and TEM, *J. Alloys Compd.* 747 (2018) 8–20.
- [15] X. Cai, Y. Xu, Microstructure, friction and wear of NbC coatings on a Fe substrate fabricated via an in situ reaction, *Surf. Coat. Technol.* 322 (2017) 202–210.
- [16] X. Cai, Y. Xu, M. Liu, L. Zhong, F. Bai, Preparation of a gradient nanostructured surface TaC layer-reinforced Fe substrate by in situ reaction, *J. Alloys Compd.* 712 (2017) 204–212.
- [17] R.O. Ritchie, The conflicts between strength and toughness, *Nat. Mater.* 10 (2011) 817–822.
- [18] J.J. Roa, E. Jimenez-Pique, C. Verge, J.M. Tarragó, A. Mateo, J. Fair, L. Llanes, Intrinsic hardness of constitutive phases in WC-Co composites: nanoindentation testing, statistical analysis, WC crystal orientation effects and flow stress for the constrained metallic binder, *J. Eur. Ceram. Soc.* 35 (2015) 3419–3425.
- [19] A. Duszová, R. Halgaš, M. Bl'anda, P. Hvizdoš, F. Lofaj, J. Dusza, J. Morgiel, Nanoindentation of WC-Co hardmetals, *J. Eur. Ceram. Soc.* 33 (2013) 2227–2232.
- [20] F. Lofaj, M. Ferdinandy, G. Cempura, J. Dusza, Nanoindentation, AFM and tribological properties of thin nc-WC/a-C coatings, *J. Eur. Ceram. Soc.* 32 (2012) 2043–2051.
- [21] N. Kadir, D.C. Faucett, S.R. Choi, N.P. Bansal, Slow-crack-growth and indentation damage in calcium magnesium, aluminosilicate (CMAS) glass from desert sand, *Ceram. Int.* 44 (2018) 2676–2682.
- [22] Y. Gu, K. Chen, R. Liu, et al., Indentation modeling study of temperature-dependent fracture toughness of brittle coating on ductile substrate based on microcrack formation theory, *Surf. Coat. Technol.* 309 (2017) 536–544.
- [23] D. Čorić, M.M. Renjo, L. Čurković, Vickers indentation fracture toughness of Y-TZP dental ceramics, *Int. J. Refract. Met. Hard Mater.* 64 (2017) 14–19.
- [24] Q. Zhan, L. Yu, F. Ye, et al., Quantitative evaluation of the decarburization and microstructure evolution of WC-Co during plasma spraying, *Surf. Coat. Technol.* 206 (2012) 4068–4074.
- [25] C.J.R.G. Oliver, E.A. Álvarez, J.L. García, Kinetics of densification and grain growth in ultrafine WC-Co composites, *Int. J. Refract. Met. Hard Mater.* 59 (2016) 121–131.
- [26] J. Pötschke, V. Richter, T. Gestrich, et al., Grain growth inhibition in ultrafine hardmetals, *Int. J. Refract. Met. Hard Mater.* 66 (2017) 95–104.
- [27] Y. Yuan, Z. Li, Growth mechanism of in-situ WC grain in Fe-Ni-W-C alloys system, *J. Alloys Compd.* 738 (2018) 379–393.
- [28] I. Borgh, P. Hedström, J. Odqvist, et al., On the three-dimensional structure of WC grains in cemented carbides, *Acta Mater.* 61 (2013) 4726–4733.
- [29] Y. Zhong, L.L. Shaw, Growth mechanisms of WC in WC-5.75 wt% Co, *Ceram. Int.* 37 (2011) 3591–3597.
- [30] X. Cai, Y. Xu, L. Zhong, M. Liu, Fracture toughness of WC-Fe cermet in W-WC-Fe composite by nanoindentation, *J. Alloys Compd.* 728 (2017) 788–796.
- [31] P. Gustafson, A thermodynamic evaluation of the C-Fe-W system, *Metall. Trans. A.* 19 (1988) 2547–2554.
- [32] Y. Ma, Y. Zhang, X. Yao, et al., Characterization of Mo surface modified Ti by indentation techniques, *Surf. Coat. Technol.* 226 (2013) 75–81.
- [33] D. Casellas, J. Caro, S. Molas, J.M. Prado, I. Valls, Fracture toughness of carbides in tool steels evaluated by nanoindentation, *Acta Mater.* 55 (2007) 4277–4286.
- [34] M. Kulka, N. Makuch, A. Piasecki, Nanomechanical characterization and fracture toughness of FeB and Fe₂B iron borides produced by gas boriding of Armco iron, *Surf. Coat. Technol.* 325 (2017) 515–532.
- [35] B. Sarma, N.M. Tikekar, K.S.R. Chandran, Kinetics of growth of superhard boride layers during solid state diffusion of boron into titanium, *Ceram. Int.* 38 (2012) 6795–6805.
- [36] M.S. Kovalchenko, Pressure sintering kinetics of tungsten and titanium carbides, *Int. J. Refract. Met. Hard Mater.* 39 (2013) 32–37.
- [37] Wei-Hsio Chen, P.K. Nayak, Hao-Tung Lin, et al., Synthesis of nanostructured tungsten carbide via metal-organic chemical vapor deposition and carburization process, *Int. J. Refract. Met. Hard Mater.* 47 (2014) 44–48.
- [38] C.M. Fernandes, A.M.R. Senos, M.T. Vieira, Versatility of the sputtering technique in the processing of WC-Fe-Ni-Cr composites, *Surf. Coat. Technol.* 206 (2012) 4915–4921.
- [39] M. Kawakami, K. Kitamura, Segregation layers of grain growth inhibitors at WC/WC interfaces in VC-doped submicron-grained WC-Co cemented carbides, *Int. J. Refract. Met. Hard Mater.* 52 (2015) 229–234.
- [40] Jolanta Prywer, Kinetic and geometric determination of the growth morphology of bulk crystals: recent developments, *Prog. Cryst. Growth Charact. Mater.* 50 (2005) 1–38.
- [41] Y. Zhong, H. Zhu, L.L. Shaw, R. Ramprasad, The equilibrium morphology of WC particles-a combined ab initio and experimental study, *Acta Mater.* 59 (2011) 3748–3757.
- [42] M.M. Renjo, L. Čurković, S. Štefančić, D. Čorić, Indentation size effect of Y-TZP dental ceramics, *Dent. Mater.* 30 (2014) 371–376.
- [43] K. Niihara, A fracture mechanics analysis of indentation-induced Palmqvist crack in ceramics, *J. Mater. Sci. Lett.* 2 (5) (1983) 221–223.
- [44] C.B. Ponton, R.D. Rawlings, Vickers indentation fracture toughness test part 1 review of literature and formulation of standardized indentation toughness equations, *Mater. Sci. Technol.* 5 (1989) 865–872.
- [45] E. Ghasali, T. Ebadzadeh, M. Alizadeh, M. Razavi, Mechanical and microstructural properties of WC-based cermets: a comparative study on the effect of Ni and Mo binder phases, *Ceram. Int.* 44 (2018) 2283–2291.